Geochemical Journal, Vol. 37, pp. 427 to 448, 2003

Geochemistry of early Mesozoic potassium-rich diorites-granodiorites in southeastern Hunan Province, South China: Petrogenesis and tectonic implications

YUEJUN WANG*, WEIMING FAN and FENG GUO

Guangzhou Institute of Geochemistry, Chinese Academy of Sciences, Guangzhou 510640, China

(*Received August 21, 2002; Accepted February 26, 2003*)

The diorites-granodiorites emplaced at *ca.* 175 Ma in southeastern Hunan tectonic-magmatic belt (SHB), South China Block (SCB), are high-K calc-alkaline. They are characterized by LREE-LILE enrichment and HFSE depletion with slight or no Eu anomalies. Age-corrected initial $^{87}Sr/^{86}Sr$ ratio spans a narrow range of 0.707962~0.710396 and $\varepsilon_{Nd}(t)$ of –6.98~–2.30. These features are significantly different from those of the neighboring other Mesozoic granitic plutons (Eu/Eu* = 0.30–0.70; $^{87}Sr/^{86}Sr > 0.710$; ε_{Nd} = –12 to –16) in South China, which have been interpreted as the remelting products of Precambrian basement. The crust anatexis cannot account for the geochemical characteristics of these diorites-granodiorites in the SHB. The partial melting of an enriched lithosphere mantle directly produced mafic-intermediate rather than acid magma, and can also not explain the geochemical and isotopic variations exhibited by these diorites-granodiorites. These diorites-granodiorites likely represent partial melting products of mantle-derived basaltic rocks, which were underplated and hybridized with old crust material at lower/middle crust level. Theoretical modeling further suggests that this hybridized source consisted of 15–30% of the lower/middle crust and 70–85% of depleted mantle-derived basaltic rocks. The occurrence of these diorite-granodiorites in southeastern Hunan province therefore marked a major intra-lithospheric extension episode during early Mesozoic.

INTRODUCTION

The South China Block (SCB) was intruded by voluminous Mesozoic granitic plutons, some of which are closely associated with large to giant multi-metal deposits (e.g., Chen and Jahn, 1998) (Fig. 1(a)). Over the past 20 years, a number of models have been postulated to explain the petrogenesis of these Mesozoic granites in SCB (e.g., Hsü *et al.*, 1990; Zhou and Li, 2000; Li, 2000). An extensional regime is now favored for the late Mesozoic tectonic evolution in the SCB (e.g., Li, 2000). However, the tectonic setting during early Mesozoic in this region remains hotly debated. Some hypotheses, such as Andean-type active continental margin, Alps-type collision belt, lithosphere subduction with underplating of mafic magma, suggested that the petrogenesis of the granites in SCB was related to the subduction/collision regime (e.g., Hsü *et al.*, 1990; Faure *et al.*, 1996; Zhou and Li, 2000, and reference therein). Others considered that they were originated from the lithospheric extension and thinning in responds to the intra-plate tectonic setting during Mesozoic (Guo *et al.*, 1997a; Li, 2000, and reference therein).

Recent studies on the Mesozoic granites have revealed that there is a Mesozoic northeast-trending high-potassium, low-T_{DM} magmatic zone ("Shi-Hang" zone, Gilder *et al.*, 1996; Li *et al.*, 1999), which is cut by Zhuguangshan Mountains in the interior of SCB (Chen and Jahn, 1998) (Fig. 1(a)). Mesozoic granodiorites-granites in the Shi-Hang zone are characterized by significantly high

*Corresponding author (e-mail: yjwang@gig.ac.cn)

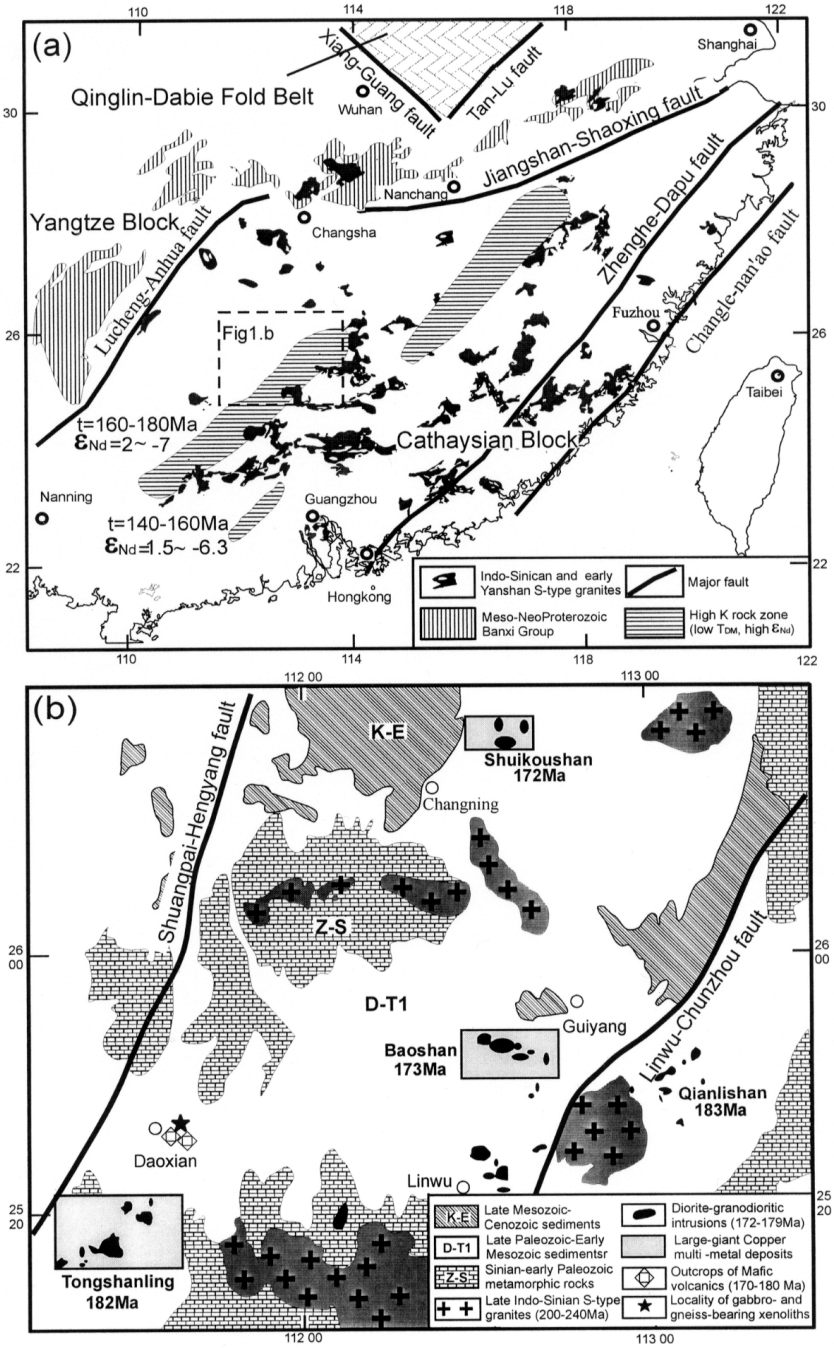

Fig. 1. (a) A simplified tectonic map of South China, showing the distribution of Mesozoic high-K, high ε_{Nd} zones (after Chen and Jahn, 1998; Zhuang et al., 1988; Li et al., 1999; Li, 2000). (b) Geologic map of southeastern Hunan tectonic-magmatic belt (SHB). The boundary between the Yangtze and Cathysian blocks is defined by the occurrence of Meso- and Neoproterozoic Banxi Group (Chen and Jahn, 1998). Mafic lavas of 170–180 Ma are from Zhao et al. (1998). The location of late Mesozoic xenoliths-bearing basalts refers to Guo et al. (1997a, b).

Sm (>8 ppm) and Nd contents (>45 ppm) with relatively high $\varepsilon_{Nd}(t)$ values (–4 to –8) and are interpreted as a result of mantle upwelling along a "paleo-rift" (Gilder *et al*., 1996). The southeastern Hunan tectonic-magmatic belt (SHB) belongs to the southern part of the Shi-Hang geochemical anomaly zone. Being an intensively deformed intracontinental belt between the Yangtze and Cathaysian blocks during Mesozoic (e.g., Hsü *et al*., 1990), this belt is also an important Mesozoic geochemical anomaly zone in the interior of SCB. In addition to voluminous Mesozoic granites in this belt (e.g., HBGMR, 1986; Chen and Jahn, 1998) (Fig. 1(a)), some early Mesozoic high-K diorites-granodiorites and mantle xenoliths-bearing mafic volcanics are present in this zone (Guo *et al*., 1997a; Zhao *et al*., 1998; Wang *et al*., 2001) (Fig. 1(b)). The magmatism might be related in temporal and spatial to underplating event identified by gabbro xenoliths (*ca*. 224 Ma) hosted by late Mesozoic basalts (Guo *et al*., 1997a). The SHB, therefore, is a crucial area for understanding early Mesozoic tectonic evolution in the SCB.

With aims to better characterize the petrogenesis and tectonic implications of early Mesozoic geochemical anomaly zone, we conducted a set of zircon U-Pb geochronological, mineralogical and geochemical studies on the diorites-granodiorites in the SHB. These diorites-granodiorites with 3–25% calcic amphibole, A/CNK = 0.79–1.19 depicted as below could be classified as I-type granitoids. They are compositionally favorable for distinguishing from the neighboring other Mesozoic granites that are predominately characterized by S-type. These diorites-granodiorites may have resulted from partial melting of underplated basaltic rocks hybridized with old crustal material at *ca*. 175 Ma. The important thermal and material transfer from mantle to crust during early Mesozoic suggests an intra-lithospheric extension setting in the SCB at that time.

Geological Setting and Petrography

The high-K diorites-granodiorites are predominately distributed in the SHB. They constitute a NE-trending tectono-magmatic zone between Chenzhou-Linwu and Hengyang-Shuangpai faults (Fig. 1(b)). Spatially, these diorites-granodiorites are closely associated with large to giant copper multi-metal deposits (e.g., HBGMR, 1986; Zhuang *et al*., 1988). From north to south in the SHB, the typical dioritic-granodioritic intrusions include Shuikoushan diorites, Baoshan and Tongshanling granodiorites. Generally, these diorites-granodiorites are of small volume and occur as veins, laccoliths, knobs and batholiths with 200–4600 m in length and 150–1600 m in width. Most of them intruded into late Paleozoic sedimentary sequences (Fig. 1(b)). For instance, Shuikoushan diorite and Baoshan granodiorite intruded into early Carboniferous sedimentary sequence, while Tongshanling granodiorite into late Permian limestone. Amphibolite, gneiss and diorite enclaves are found in Tongshanling, but absent in other two intrusions.

Lithologically, Baoshan and Tongshanling intrusions comprise predominately biotite granodiorites whereas Shuikoushan intrusion contains biotite diorites and quartz diorites. These diorites-granodiorites show subhedral granular textures of mediate grain sizes (2–5 mm) with partial porphyritic fabrics in some samples. The phenocrysts are commonly constituted by plagioclase, quartz and alkali feldspar, and the matrix is mainly composed of fine-grained plagioclase, quartz and a few biotite, amphibole and opaque oxides. The rocks contain 35–50% plagioclase, 5–25% alkali feldspar, 10–35% quartz, 5–15% biotite, 3–25% amphibole and minor amounts of euhedral sphene, apatite, zircon, Fe-Ti oxides and allanite. Plagioclase phenocrysts display optical zonation, and tend to be euhedral to subhedral with the size of 2–5 mm. The alkali feldspar is microcline, and contains abundant perthite as blebs and stringers. Hornblende exhibits brown-light and green subhedral-anhedral polychroism. Variation in mineral contents is somewhat correlated with that of SiO_2 contents in these intrusions. Shuikoushan diorites-granodiorites (SiO_2 = 60.0–65.1%) have higher

proportion of biotite and hornblende but less K-feldspar and quartz than that of Baoshan and Tongshanling granodiorites (SiO_2 = 63.3–68.2%).

Analytical Techniques

Zircons were finally separated and concentrated by heavy liquid, and isodynamic magnetic separators and were then handpicked under a binocular microscope. Only those idiomorphic zircon grains free of inclusions and cracks have been selected for U-Pb dating. Zircon grains were digested in a 0.25-ml Teflon capsule and spiked by the combination-bombs with ^{205}Pb-^{235}U-spike mixture. Four to ten grains for each separate sample were selected for U-Pb isotopic analyses. The procedure is after Krogh's (1973). The initial common Pb is corrected by model of Stacey and Kramers (1975) and whole procedure blank was 0.050 ng for Pb and 0.002 ng for U. U-Pb abundance and their isotopic ratios were determined using a mass-spectrometer VG 354 at Tianjin Institute of Geology and Mineral Resources, Chinese Ministry of Land and Resources (MLR). All U-Pb analyses were done using an ion-counting Daly detector in peak hopping mode. Data procession was performed using the PBDAT and plotted by ISOPLOT software. The results are given in Table 1.

The chemical compositions of single minerals were performed on a JCXA-733 Microscan Microprobe (0.2 μA, 20 kV) at the Institute of Geochemistry, Chinese Academy of Sciences (CAS). Representative mineral compositions are given in Table 2. The hornblende and biotite compositions listed in Table 2 are the mean values of 3–5 individual spots from several neighboring grains.

Major oxide contents were analyzed at the Hubei Institute of Geology and Mineral Resource, MLR, by a wavelength X-ray fluorescence spectrometry with analytical errors better than 2%. FeO content in sample is solely analyzed by a wet chemical method. Trace element analysis was performed at the Guangzhou Institute of Geochemistry, CAS by an inductively coupled plasma mass spectrometry (ICP-MS). Detailed analytical procedure is referred from Liu *et al.* (1996). Reproductivity is better than 95% with general analytical error less than 5%.

Sr and Nd isotopic ratios were measured by a VG 354 mass-spectrometer at Institute of Geology and Geophysics, CAS. The ratios were normalized to $^{86}Sr/^{88}Sr = 0.1194$ and $^{146}Nd/^{144}Nd = 0.7219$, respectively. The whole procedure blanks are lower than 5×10^{-10} g for Sr and 5×10^{-11} g for Nd. Thirteen analyses of standard La Jolla gave $^{143}Nd/^{144}Nd = 0.511962 \pm 10$, and two analyses of BCR-1 gave $^{143}Nd/^{144}Nd$ ratios of 0.512626 ± 9. Six analyses of NBS 987 gave $^{87}Sr/^{86}Sr = 0.710265 \pm 12$, and two analyses of NBS607 gave $^{87}Sr/^{86}Sr = 1.20032 \pm 3$ (1 s.d.). $^{87}Rb/^{86}Sr$ and $^{147}Sm/^{144}Nd$ ratios were calculated using the Rb, Sr, Sm and Nd abundances measured by ICP-MS. During the course of this study within-run errors of precision are estimated to be better than 0.000015 for $^{86}Sr/^{88}Sr$ and $^{146}Nd/^{144}Nd$ in the 95% confidence level. $^{143}Nd/^{144}Nd$ and $^{147}Sm/^{144}Nd$ ratios of CHUR at the present time used for calculating ε_{Nd} value are 0.512638 and 0.1967 respectively. Major, trace elements and Sr-Nd isotopic ratios are listed in Table 3.

Results

Zircon U-Pb dating

All zircon grains for U-Pb dating are light brown, prismatic and transparent with well-developed crystal faces, indicating that they are predominately magmatic (Wang *et al.*, 2001). Four zircon grains from a Baoshan granodiorite are plotted on the concordia line with a mean $^{206}Pb/^{238}U$ apparent age of 173.3 ± 1.9 Ma (*MSWD* = 0.051) (Fig. 2(a)). Three zircon grains from a Shuikoushan diorite are also on the concordia line (Fig. 2(b)), yielding a mean $^{206}Pb/^{238}U$ apparent age of 172.3 ± 1.6 Ma (*MSWD* = 0.181). These diorites-granodiorites in SHB were generated at 800–850°C discussed in Subsection 4.2, whereas the closure temperature of zircon U-Pb isotopic system is generally 650–700°C. Therefore this age is considered as the best estimate of its crystalli-

Table 1. U-Pb isotopic analyses of grained zircon from the diorites-granodiorites in SHB

Sample description			Concentration		Com. Pb (ng)	Isotopic atom ratio					Apparent age (Ma)		
Sample	No.	Weight (μg)	U ($\mu g \cdot g^{-1}$)	Pb ($\mu g \cdot g^{-1}$)		$^{206}Pb/^{204}Pb$	$^{208}Pb/^{206}Pb$	$^{206}Pb/^{238}U$	$^{207}Pb/^{235}U$	$^{207}Pb/^{206}Pb$	$^{206}Pb/^{238}U$	$^{207}Pb/^{235}U$	$^{207}Pb/^{206}Pb$
Tongshanling granodiorite													
	1	15	1248	37	0.041	839	0.08139	0.02818 (40)	0.1938 (48)	0.04987 (93)	179.1 (2.5)	179.8 (4.3)	189.1 (43)
	2	20	942	28	0.025	1339	0.11060	0.02810 (38)	0.1927 (40)	0.04973 (71)	178.7 (2.4)	178.9 (3.4)	182.2 (33)
	3	20	1577	52	0.087	727	0.08027	0.03086 (23)	0.2386 (26)	0.05608 (41)	195.9 (1.4)	217.3 (2.1)	455.6 (16)
	4	20	979	46	0.044	1205	0.07523	0.04584 (37)	0.4701 (48)	0.07438 (41)	289.0 (2.3)	391.3 (3.4)	1052 (11)
	5	20	755	45	0.017	2848	0.09760	0.05603 (32)	0.8280 (52)	0.10720 (3)	351.4 (2.0)	612.5 (3.2)	1752 (4)
	6	20	1930	60	0.059	1274	0.07157	0.03050 (19)	0.2214 (21)	0.05265 (33)	193.7 (1.0)	203.1 (1.7)	313.8 (14)
	7	20	861	28	0.010	3659	0.08119	0.03256 (26)	0.2466 (28)	0.05492 (39)	206.5 (1.6)	223.8 (2.3)	409.2 (16)
	8	20	1374	47	0.029	2033	0.08255	0.03359 (32)	0.2648 (45)	0.05717 (78)	213.0 (2.0)	238.5 (3.7)	498.0 (30)
	9	15	2542	97	0.096	848	0.09088	0.03603 (22)	0.2931 (28)	0.05899 (42)	228.2 (1.4)	261.0 (2.2)	566.9 (16)
	10	15	670	27	0.008	2691	0.1206	0.03821 (44)	0.4069 (57)	0.07725 (54)	241.7 (2.8)	346.7 (4.0)	1128 (14)
Shuikoushan diorite													
	1	20	997	31	0.049	715	0.1782	0.02708 (35)	0.1850 (38)	0.04955 (78)	172.2 (2.3)	172.4 (3.2)	174.0 (33)
	2	10	1536	59	0.150	195	0.1888	0.02716 (43)	0.1861 (48)	0.04970 (91)	172.7 (2.8)	173.3 (4.7)	180.8 (43)
	3	20	484	18	0.081	222	0.1810	0.02700 (69)	0.1846 (75)	0.04958 (143)	171.8 (4.4)	172.0 (6.5)	175.5 (67)
	4	20	992	37	0.120	324	0.1570	0.03007 (35)	0.2560 (46)	0.06176 (77)	191.0 (2.2)	231.5 (3.7)	666 (27)
Baoshan granodiorite													
	1	20	247	9	0.038	242	0.1671	0.02714 (135)	0.1858 (148)	0.04964 (280)	172.7 (8.6)	173.0 (12.6)	178.0 (130)
	2	20	560	17	0.013	1505	0.1686	0.02711 (51)	0.1853 (54)	0.04957 (100)	172.4 (3.3)	172.6 (4.7)	174.9 (47)
	3	20	744	27	0.130	220	0.1426	0.02734 (48)	0.1887 (75)	0.05006 (167)	173.9 (3.0)	175.5 (6.4)	198.0 (77)
	4	20	455	14	0.015	1046	0.1451	0.02733 (63)	0.1872 (66)	0.04968 (119)	173.8 (4.0)	174.3 (5.6)	180.3 (56)

$^{206}Pb/^{204}Pb$ is corrected for the whole procedure laboratory blank (Pb = 0.050 ng and U = 0.002 ng) and diluent. Other Pb isotopic ratios are radioactive Pb isotopic ratio in these expressions. The common Pb was corrected by the Stacey and Kramers' (1975) method. The number in bracket (2σ) in the column of isotopic atom ratio and of apparent age (Ma) is the analytical errors for U and Pb isotopic ratios and errors to the apparent ages, respectively. e.g.: 0.1861(48) in the column of isotopic atom ratio shows 0.1861 ± 0.0048(2σ), and 179.1(2.5) in the column of apparent age (Ma) is 179.1 ± 2.5 Ma.

zation age. The fourth zircon is plotted below the concordia line with a $^{207}Pb/^{206}Pb$ apparent age of 666 ± 27 Ma. It is unclear for the exact geological meaning of the older apparent age. It is inferred that the zircon has possibly rudimental core from crust basement. Two zircon grains from a Tongshanling granodiorite are plotted on the concordia line and yield a mean $^{206}Pb/^{238}U$ apparent age of 178.9 ± 1.7 Ma (*MSWD* = 0.181). The others from the Tongshanling sample are plotted

Table 2. Representative microprobe analyses of hornblende, plagioclase and biotite

Intrusion	Mineral	SiO_2	TiO_2	Al_2O_3	FeO*	MnO	MgO	CaO	Na_2O	K_2O	Total	Si	Al^{VI}	Al^{IV}	A site	Pressure
TSHL	Hbc	48.6	0.73	7.19	17.5	0.62	11.6	9.96	1.14	0.51	97.9	7.20	0.80	0.45	0.31	2.96
	Hbr	48.1	0.86	6.60	17.3	0.68	11.3	11.0	0.98	0.64	97.5	7.18	0.82	0.34	0.34	2.51
	Hb	47.5	0.85	6.57	18.4	0.95	11.1	9.87	1.17	0.45	96.9	7.16	0.84	0.33	0.36	2.55
	Hb	46.7	1.14	7.45	19.3	0.65	11.6	8.77	1.33	0.43	97.3	7.02	0.98	0.34	0.43	3.27
	Hb	49.9	0.48	8.30	19.5	0.91	11.7	7.55	1.33	0.19	97.1	7.21	0.79	0.62	0.22	3.71
BSH	Hb	48.5	0.63	8.77	19.1	1.02	11.0	7.44	1.11	0.18	97.8	7.16	0.84	0.68	0.30	4.25
	Hb	47.4	1.05	7.09	19.8	0.79	11.5	7.07	1.48	0.24	96.6	7.15	0.85	0.41	0.32	2.99
SHKSH	Hb	48.8	0.78	8.75	18.1	0.87	11.6	7.25	1.34	0.27	97.9	7.17	0.83	0.68	0.19	4.19
	Hb	49.1	0.92	7.51	19.2	1.04	10.8	6.59	1.52	0.27	97.0	7.31	0.69	0.62	0.17	3.26
	Hb	51.1	0.44	7.05	17.9	0.85	12.1	7.13	0.82	0.10	97.6	7.45	0.55	0.67	0.09	2.76
Intrusion	Mineral	SiO_2	TiO_2	Al_2O_3	FeO*	MnO	MgO	CaO	Na_2O	K_2O	Total	Si	Al^T	An	Ab	Or
TSHL	Plc	60.9	0.06	22.3	0.16	0.02	0.01	7.96	7.23	0.29	99.0	2.75	1.19	0.37	0.62	0.02
	Plr1	61.7	0.02	22.2	0.14	0.15	n.d.	7.03	7.42	0.42	99.1	2.78	1.18	0.33	0.64	0.02
	Plr2	62.8	n.d.	21.9	0.09	0.07	0.15	6.12	8.10	0.34	99.5	2.81	1.15	0.29	0.69	0.02
	Plc	62.7	0.06	21.5	n.d.	n.d.	n.d.	5.32	9.51	0.27	99.4	2.81	1.14	0.23	0.76	0.01
	Plr1	61.5	n.d.	22.6	0.13	n.d.	n.d.	5.64	9.12	0.14	99.2	2.77	1.20	0.25	0.74	0.01
	Plr2	62.5	0.03	21.9	0.31	0.11	0.03	5.29	9.34	0.10	99.7	2.8	1.16	0.24	0.76	0.01
	Plr3	61.8	0.05	21.7	0.10	n.d.	0.38	5.04	9.57	0.19	99.1	2.78	1.15	0.22	0.77	0.01
	Plc	57.6	n.d.	26.1	0.44	0.05	0.07	7.80	7.01	0.09	99.1	2.61	1.39	0.38	0.62	0.01
	Plr1	58.5	0.05	24.5	0.09	0.01	n.d.	7.09	7.01	0.02	97.4	2.68	1.32	0.36	0.64	0.00
	Plr2	59.0	n.d.	25.8	0.30	0.03	n.d.	7.57	6.92	0.07	99.6	2.64	1.36	0.37	0.62	0.00
	Plr3	58.8	n.d.	25.5	0.28	n.d.	0.15	7.56	7.10	0.16	99.5	2.64	1.35	0.36	0.63	0.01
	Plr4	60.3	0.03	24.9	0.21	0.00	0.01	7.39	7.56	0.18	101.0	2.68	1.30	0.34	0.65	0.01
	Pl	60.5	n.d.	25.1	0.36	n.d.	n.d.	6.69	6.89	0.09	99.7	2.7	1.32	0.34	0.65	0.01
SHKSH	Plc	59.9	n.d.	26.2	0.16	n.d.	n.d.	7.27	6.83	0.09	100.0	2.65	1.37	0.37	0.63	0.01
	Plr1	62.5	0.03	22.7	0.08	0.02	0.03	4.29	9.34	0.10	99.1	2.81	1.21	0.24	0.78	0.01
	Plr2	63.8	n.d.	23.5	0.03	n.d.	n.d.	4.26	7.83	0.10	99.8	2.81	1.22	0.23	0.77	0.01
	Plr3	62.4	0.03	23.6	0.00	n.d.	n.d.	4.63	8.13	0.09	98.8	2.78	1.24	0.24	0.76	0.01
	Plr4	62.6	0.06	23.5	0.10	0.06	0.05	4.46	8.81	0.02	99.7	2.78	1.23	0.22	0.78	0.00
	Pl	62.4	n.d.	24.5	0.09	n.d.	0.04	4.29	7.74	0.14	99.4	2.77	1.28	0.23	0.76	0.01
Intrusion	Mineral	SiO_2	TiO_2	Al_2O_3	FeO*	MnO	MgO	CaO	Na_2O	K_2O	Total	Si	Al^T			
TSHL	Bt	38.8	2.67	11.9	26.5	0.39	9.52	0.04	n.d.	7.13	97.0	9.54	2.22			
	Bt	37.4	4.20	11.9	22.0	0.42	11.2	0.02	n.d.	9.71	97.0	9.45	2.17			
BSH	Bt	37.1	3.40	12.2	23.1	0.53	10.5	0.03	0.29	8.78	96.0	9.39	2.23			
SHKSH	Bt	38.8	2.77	12.2	26.0	0.44	9.11	0.06	0.18	8.05	96.6	9.46	2.25			
	Bt	37.7	3.53	12.7	24.9	0.43	11.6	0.02	0.37	4.11	95.3	9.61	2.28			

FeO is the total content of FeO + Fe_2O_3. c refer to core and r1, r2, r3 and r4 to rims of minerals from core to edge. n.d. not determined. Hb, Pl and Bt are hornblende, plagioclase and biotite, respectively. TSHL, BSH and SHKSH are for Tongshanling, Baoshan and Shuikoushan intrusions, respectively. Pressure estimates using the equation from Schmidt (1992).*

below the concordia line but constitute a well-defined regression line (*MSWD* = 5.5) with the upper intercept age of 1746 ± 197 Ma and the lower intercept age of 181.7 ± 8.8 Ma (Fig. 2(c)).

Collectively, the emplacement of these studied diorites-granodiorites took place within a limited time interval between 172–182 Ma, and they have an identical crystallization age within error bar. Some of zircon grains from the Tongshanling granodiorite give the upper intercept age of 1746 ± 197 Ma (and $^{207}Pb/^{206}Pb$ apparent ages), significantly greater than 182 Ma. This age is somewhat similar to the metamorphic age of the gneiss xenoliths (1964 ± 164 Ma) in the SHB (Guo *et al.*, 1997b) and thus can be attributed to the inherited zircons extracted from Precambrian lower/middle crust (LC/MC). The occurrence of inherited zircons implies that the dioritic-granodioritic magma in the SHB might have been contaminated by old crust material during magma ascent. Alternatively, the metamorphic basement had an important contribution to their source (Wang *et al.*, 2001).

Table 3. The analyses of the element-isotope from the diorites-granodiorites in SHB

Sample	TSD-1	TSD-2	TSD-4	TSD-9	JYT-3	JYT-10	JYT-14	TSX-1	TSX-5	TSX-6	TSX-7
SiO_2	66.58	65.52	67.20	65.42	68.16	66.85	68.18	67.18	66.18	67.02	64.78
TiO_2	0.41	0.48	0.42	0.49	0.42	0.45	0.43	0.45	0.45	0.47	0.48
Al_2O_3	15.86	15.70	14.97	15.84	14.36	14.86	14.51	15.26	15.70	15.26	15.99
FeO	2.54	2.86	2.21	3.08	2.53	3.13	3.03	2.98	3.33	3.38	3.62
Fe_2O_3	0.38	0.62	0.48	0.30	0.33	0.31	0.21	0.32	0.14	0.18	0.18
CaO	4.06	4.47	3.93	4.61	2.90	3.37	3.24	3.66	4.20	4.47	4.61
MgO	1.30	1.39	1.11	1.39	1.09	1.33	1.32	2.19	1.58	1.86	1.81
K_2O	4.01	3.54	4.02	4.20	4.37	3.75	4.29	4.08	4.21	3.34	3.52
Na_2O	2.94	3.12	3.02	3.18	2.50	2.86	2.78	2.96	3.21	3.12	3.23
P_2O_5	0.13	0.17	0.16	0.19	0.16	0.17	0.17	0.14	0.15	0.15	0.17
MnO	0.06	0.06	0.06	0.02	0.08	0.10	0.09	0.09	0.09	0.09	0.04
LOS	1.82	1.92	2.12	1.04	2.88	2.59	1.54	0.98	0.70	1.10	1.30
Total	100.09	99.85	99.70	99.76	99.78	99.77	99.79	100.29	99.94	100.44	99.73
Sc	6.93	8.06	7.04	7.64	7.99	8.88		7.96	9.01	8.52	9.04
Co	8.39	10.1	8.51	7.83	5.72	8.11		8.21	11.1	8.75	8.92
Ni	4.77	5.05	5.22	5.22	6.96	13.0		5.24	5.83	6.50	6.61
Rb	187	127	163	203	211	184		196	165	151	135
Sr	198	299	299	299	291	334		317	335	293	317
Y	21.2	21.7	19.3	24.5	19.3	26.1		20.5	25.7	23.4	21.8
Zr	112	129	127	133	140	147		86.1	138	133	126
Nb	15.6	16.9	16.8	17.1	16.7	17.8		15.4	15.7	16.0	16.9
Ba	505	614	632	546	728	575		720	698	475	658
Hf	3.87	4.24	4.21	4.36	4.76	4.91		3.11	4.66	4.49	4.16
Ta	1.83	1.67	1.84	1.72	1.79	2.00		1.60	1.84	1.63	1.63
Th	11.7	22.3	20.3	16.3	14.3	15.0		15.7	10.7	13.5	14.5
U	5.27	7.87	6.83	5.15	5.51	7.69		6.80	6.35	7.73	4.25
La	14.9	35.8	37.1	33.5	29.4	25.2		21.6	19.3	19.1	33.8
Ce	28.7	66.9	68.1	64.9	55.5	48.7		41.3	36.9	37.8	61.5
Pr	3.70	7.82	8.03	7.57	6.13	5.70		5.19	4.79	4.76	7.33
Nd	13.9	28.4	27.7	27.1	22.8	21.1		19.3	18.3	18.1	26.0
Sm	3.36	5.39	5.16	5.35	4.24	4.94		4.16	4.28	4.16	4.98
Eu	0.87	1.21	1.09	1.18	1.06	1.11		1.14	1.19	1.08	1.30
Gd	3.31	4.75	4.29	4.87	3.45	4.14		3.85	4.29	4.16	4.44
Tb	0.53	0.67	0.62	0.69	0.57	0.67		0.58	0.67	0.63	0.63
Dy	3.41	3.98	3.59	4.27	3.24	4.23		3.59	4.32	4.02	3.82
Ho	0.72	0.80	0.71	0.86	0.61	0.79		0.73	0.90	0.84	0.80
Er	2.21	2.35	2.07	2.58	1.74	2.43		2.18	2.76	2.47	2.38
Tm	0.34	0.34	0.30	0.38	0.26	0.41		0.32	0.42	0.37	0.35
Yb	2.33	2.35	2.00	2.57	1.79	2.60		2.19	2.94	2.55	2.34
Lu	0.36	0.34	0.29	0.39	0.29	0.42		0.33	0.44	0.38	0.34
La/Sm	4.42	6.64	7.19	6.27	6.93	5.11		5.19	4.15	4.95	6.79
Ce/Yb	12.3	28.5	34.0	25.3	31.0	18.7		18.9	12.6	14.8	26.3
$^{147}Sm/^{144}Nd$	0.160	0.126	0.124	0.131				0.143	0.156	0.152	0.127
$^{87}Rb/^{86}Sr$	2.730	1.227	1.615	1.972				1.794	1.429	1.498	1.240
$^{144}Nd/^{143}Nd(i)$	0.512314	0.512219	0.512277	0.512371				0.512458	0.512421	0.512437	0.512350
(2σ)	(9)	(8)	(9)	(9)				(10)	(10)	(10)	(12)
$^{87}Sr/^{86}Sr(i)$	0.715813	0.713520	0.714480	0.713249				0.712528	0.712142	0.712439	0.712108
(2σ)	(19)	(13)	(13)	(11)				(20)	(20)	(15)	(16)
$^{144}Nd/^{143}Nd(t)$	0.512126	0.512071	0.512132	0.512217				0.512290	0.512239	0.512258	0.512201
$\varepsilon_{Nd}(t)$	–5.49	–6.57	–5.37	–3.71				–2.30	–3.30	–2.91	–4.04
$^{87}Sr/^{86}Sr(t)$	0.708866	0.710396	0.710370	0.708229				0.707962	0.708506	0.708627	0.708952

Table 3. (continued)

Sample	JHT-2	JHT-8	JHT-13	BSH-1	BSH-2	BSH-3	BSH-4	BSH-5	BSH-6	BSH-7
SiO_2	66.67	65.87	66.76	66.58	65.40	68.01	64.46	68.80	64.50	63.28
TiO_2	0.50	0.53	0.45	0.37	0.41	0.36	0.45	0.43	0.48	0.44
Al_2O_3	15.14	15.02	15.14	14.39	14.61	13.67	14.68	13.73	15.12	15.19
FeO	3.07	3.47	2.90	1.93	2.25	1.83	2.63	1.97	2.73	2.10
Fe_2O_3	0.62	0.24	0.43	0.38	0.75	0.71	0.66	0.70	1.05	0.56
CaO	3.69	3.84	3.59	4.65	3.75	3.68	2.89	2.33	3.57	5.96
MgO	1.46	1.62	1.36	1.14	2.23	1.29	2.76	1.55	3.06	2.21
K_2O	3.79	4.20	3.91	4.20	4.42	4.61	4.22	4.81	4.39	4.44
Na_2O	2.89	2.81	3.01	2.62	2.81	2.75	2.82	2.83	2.99	2.22
P_2O_5	0.19	0.20	0.17	0.18	0.14	0.17	0.15	0.15	0.16	0.15
MnO	0.09	0.09	0.09	0.13	0.05	0.11	0.04	0.08	0.06	0.10
LOS	1.68	1.89	1.98	3.25	3.18	2.52	3.72	2.40	2.04	3.78
Total	99.79	99.78	99.79	99.82	100.00	99.71	99.64	99.78	100.15	100.48
Sc	9.18	10.1	10.9	7.78	9.18	7.71	5.99	7.79	10.4	2.67
Co	9.44	10.5	9.83	6.98	5.47	4.75	7.69	5.42	8.20	6.62
Ni	10.4	18.6	11.1	7.19	2.58	2.88	3.78	14.3	3.39	3.06
Rb	183	201	188	165	183	201	189	207	186	173
Sr	362	387	363	115	79.8	129	65.1	107	74.8	79.7
Y	29.8	26.3	29.8	24.4	23.8	24.4	22.9	18.7	21.8	13.3
Zr	162	160	139	107	111	108	107	105	134	113
Nb	20.1	19.0	18.9	16.0	16.3	16.7	17.3	16.9	18.7	16.4
Ba	541	803	594	563	682	591	520	639	753	493
Hf	5.41	4.94	4.06	3.88	3.47	3.98	3.97	4.01	4.84	4.01
Ta	2.03	1.53	1.81	1.33	1.45	1.56	1.45	1.47	1.49	1.35
Th	15.7	11.5	14.2	14.0	14.67	16.2	15.4	15.4	17.9	16.21
U	7.50	4.13	6.37	4.98	3.25	2.90	4.48	3.28	4.63	3.29
La	28.0	27.0	22.2	32.3	27.1	32.1	28.7	29.4	35.6	25.8
Ce	51.8	50.9	41.7	60.8	53.0	62.5	61.1	57.0	66.1	58.5
Pr	6.16	5.89	4.90	6.71	6.72	7.03	7.05	6.37	8.01	6.65
Nd	23.7	23.5	18.7	25.2	24.8	26. 6	25.8	24.1	28.6	24.3
Sm	4.93	5.21	4.37	5.27	5.11	5.12	5.19	4.50	5.46	4.83
Eu	1.24	1.25	0.94	1.22	1.28	1.15	1.15	0.94	1.22	1.17
Gd	4.67	4.54	4.16	4.56	4.67	4.61	4.54	3.81	4.51	4.27
Tb	0.81	0.75	0.66	0.68	0.69	0.63	0.66	0.50	0.65	0.62
Dy	4.90	4.38	4.05	4.18	4.26	4.34	3.98	3.35	3.83	3.72
Ho	0.97	0.86	0.84	0.85	0.87	0.83	0.81	0.61	0.79	0.74
Er	2.95	2.61	2.60	2.44	2.68	2.57	2.46	2.03	2.42	2.23
Tm	0.42	0.37	0.36	0.40	0.40	0.40	0.38	0.34	0.37	0.33
Yb	2.87	2.41	2.54	2.578	2.94	2.72	2.64	2.16	2.62	2.28
Lu	0.43	0.35	0.38	0.37	0.45	0.40	0.40	0.33	0.40	0.34
La/Sm	5.68	5.18	5.07	6.13	5.31	6.27	5.52	6.53	6.51	5.33
Ce/Yb	18.1	21.1	16.4	22.0	18.0	23.0	23.2	26.4	25.2	25.7
$^{147}Sm/^{144}Nd$					0.137		0.134		0.127	0.132
$^{87}Rb/^{86}Sr$					6.633		8.401		7.207	6.301
$^{144}Nd/^{143}Nd(i)$					0.512213		0.512253		0.512227	0.512263
(2σ)					(12)		(9)		(9)	(9)
$^{87}Sr/^{86}Sr(i)$					0.725834		0.730297		0.727253	0.725769
(2σ)					(14)		(15)		(13)	(12)
$^{144}Nd/^{143}Nd(t)$					0.512058		0.512101		0.512084	0.512113
$\varepsilon_{Nd}(t)$					–6.98		–6.13		–6.47	–5.90
$^{87}Sr/^{86}Sr(t)$					0.709519		0.709635		0.709526	0.710272

Table 3. (continued)

Sample	BSH-8	SKS-1	SKS-3	SKS-5	SKS-6	SKS-7	SKS-8	SKS-9	Gneiss(4)	97Hu-30
SiO_2	63.42	60.26	60.00	64.67	65.05	60.88	64.53	61.48	68.65	45.56
TiO_2	0.50	0.78	0.81	0.68	0.70	0.77	0.70	0.74	0.60	0.49
Al_2O_3	15.48	17.00	17.51	15.91	15.68	16.28	15.67	16.43	13.41	14.88
FeO	2.48	2.96	3.00	2.57	2.63	2.62	2.53	2.41	0.74	1.90
Fe_2O_3	1.71	2.29	2.36	2.32	1.82	2.20	2.39	2.01	3.60	5.50
CaO	5.42	4.30	2.98	2.77	2.73	4.27	2.73	4.22	1.80	16.13
MgO	2.53	3.39	3.29	2.34	2.59	3.01	2.59	3.05	2.72	8.58
K_2O	4.66	3.94	3.36	3.30	3.30	3.48	3.35	3.84	3.73	1.01
Na_2O	2.21	2.14	2.67	2.92	2.80	2.98	2.72	2.90	1.77	1.45
P_2O_5	0.19	0.41	0.35	0.38	0.38	0.37	0.38	0.36	0.13	0.06
MnO	0.08	0.06	0.05	0.04	0.05	0.06	0.05	0.07	0.07	0.14
LOS	1.84	2.68	3.40	1.85	2.05	2.54	2.17	1.82	2.42	4.01
Total	100.52	100.21	99.78	99.75	99.78	99.46	99.81	99.33	99.40	99.83
Sc		11.9	13.0	16.0	16.9	18.9	16.6	19.2	12.9	
Co		13.4	19.4	11.3	10.6	10.1	11.6	9.48	16.0	41.8
Ni		13.2	11.9	14.9	14.1	11.8	15.3	9.89	16.4	
Rb		136	189	142	137	84.0	138	77.6	124	35.5
Sr		78.6	99.6	399	401	309	379	306	279	654
Y		14.3	12.6	14.6	18.1	19.3	18.9	19.6	34.1	11.6
Zr		146	126	111	130	139	133	133	219	33.0
Nb		15.9	16.2	16.6	16.4	14.2	17.1	14.3	13.8	3.30
Ba		276	400	465	492	257	491	392	909	284
Hf		7.48	4.10	3.92	4.58	5.79	4.49	4.29	6.42	1.70
Ta		0.97	0.99	1.01	1.04	0.89	1.06	0.89	1.13	0.43
Th		10.5	8.49	15.7	15.0	13.1	15.4	12.5	17.9	13.3
U		3.27	2.18	3.16	3.15	2.70	3.29	2.43	2.40	0.40
La		21.1	31.8	48.8	54.4	46.9	48.9	46.5	42.3	4.24
Ce		54.9	63.4	86.5	101	88.2	92.0	84.1	82.8	10.5
Pr		5.52	7.80	9.43	11.3	10.7	10.4	10.4	9.32	1.39
Nd		20.9	28.5	34.8	42.7	38.2	38.3	37.8	37.5	6.20
Sm		4.36	5.07	6.07	7.97	8.61	6.99	8.66	6.93	1.73
Eu		1.07	1.25	1.78	1.94	2.32	1.95	2.43	1.44	0.72
Gd		3.95	4.02	4.54	5.80	5.79	5.66	5.99	6.19	2.08
Tb		0.52	0.51	0.61	0.75	0.73	0.73	0.77	0.96	0.34
Dy		2.98	2.79	2.91	3.90	3.88	3.95	4.06	5.76	2.13
Ho		0.58	0.53	0.53	0.64	0.74	0.73	0.76	1.34	0.41
Er		1.70	1.53	1.48	1.71	2.08	1.95	2.08	3.09	1.17
Tm		0.24	0.21	0.20	0.26	0.27	0.27	0.27	0.51	0.18
Yb		1.59	1.40	1.22	1.44	1.74	1.64	1.79	3.33	1.06
Lu		0.25	0.21	0.18	0.21	0.26	0.27	0.26	0.53	0.16
La/Sm		4.80	6.27	7.63	6.82	5.45	6.99	5.35	6.10	2.45
Ce/Yb		34.5	45.3	70.9	70.0	50.7	56.1	47.0	24.9	59.9
$^{147}Sm/^{144}Nd$		0.138	0.118			0.150		0.152		0.1808
$^{87}Rb/^{86}Sr$		5.013	5.516			0.785		0.735		
$^{144}Nd/^{143}Nd(i)$		0.512253	0.512219			0.512272		0.512280		0.512267
(2σ)		(8)	(12)			(10)		(11)		
$^{87}Sr/^{86}Sr(i)$		0.721045	0.723729			0.711467		0.711527		
(2σ)		(20)	(25)			(20)		(14)		
$^{144}Nd/^{143}Nd(t)$		0.512097	0.512086			0.512103		0.512109		
$\varepsilon_{Nd}(t)$		–6.23	–6.46			–6.12		–6.01		
$^{87}Sr/^{86}Sr(t)$		0.708787	0.710239			0.709548		0.709729		

TSD, TSX, JYT and JHT are from Tongshanling granodiorites (t = 179 Ma). BSH and SKS are from Baoshan (t = 172 Ma) and Shuikoushan diorites-granodiorites (t = 173 Ma), respectively. Gneiss (4) refers to the average of four gneiss xenoliths (from Guo et al., 1997b; Li, 1990) and 97Hu-30 is granulite xenolith in SHB (from Kong et al., 2000).

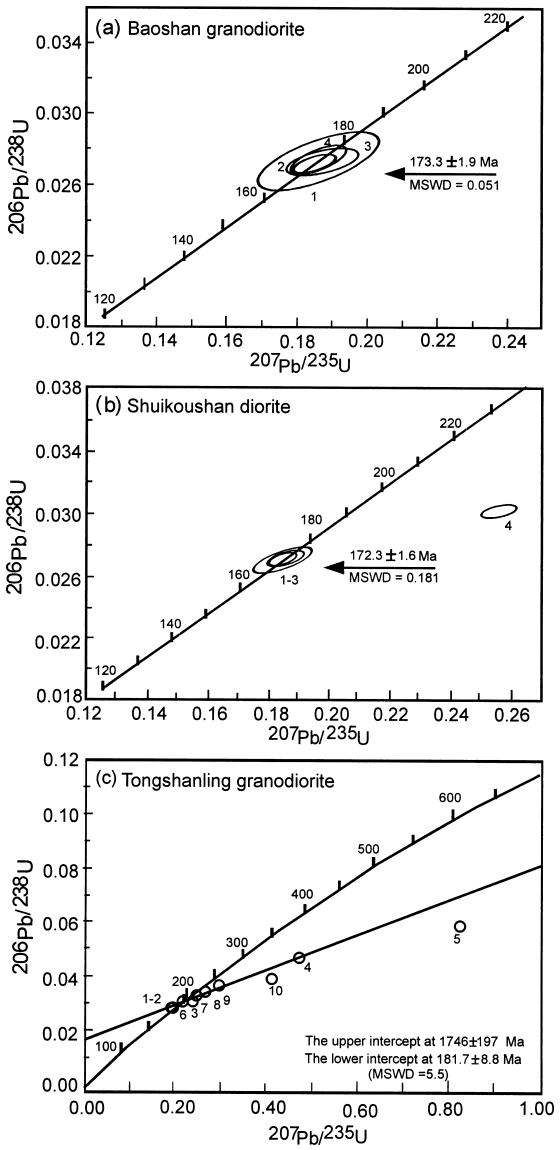

Fig. 2. Grain zircon U-Pb dating of Shoukoushan diorite and Banshan and Tongshanling granodiorites in the SHB.

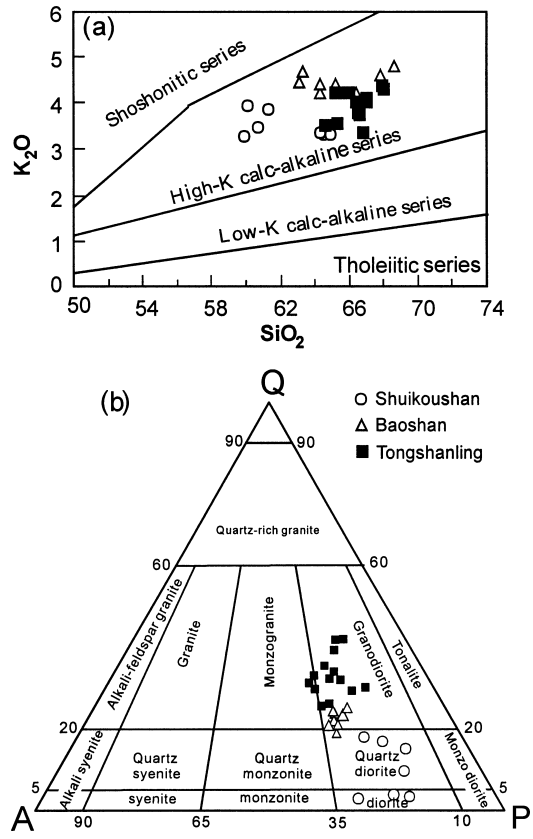

Fig. 3. (a) SiO_2 vs. K_2O plots (after Morrison, 1980) and (b) QAP diagram (after Steckeisen, 1973). Q, A, P are quartz, alkali feldspar and plagioclase contents in thin section, respectively. The symbols in (b) are applied to (a).

Mineralogy

Plagioclases in diorites and/or granodiorites from different plutons have uniform chemical compositions (Table 2). They generally show a high SiO_2 (57.6~63.8 wt%), Al_2O_3 (21.7~26.7 wt%) and Na_2O (5.9~9.6 wt%) contents and a low CaO (4.3~8.4 wt%), K_2O (<1.0 wt%) contents (Table 2). Subsequently, they are low in An (An = 22~38). Some plagioclase phenocrysts show normal zoning with a relatively low An percentage in rim.

Amphibole and biotite are the most common mafic minerals in these rocks. Biotite is highly aluminous [Al/(Al+Si+Mg+Fe) = 0.22–0.24] and ferrous [Fe/(Fe+Mg) = 0.50–0.62]. The TiO_2 content ranges from 2.63% to 3.57% (Table 2). The amphiboles are mainly hornblendes with a few artinolitic hornblendes on the A site versus Si^{VI} diagram (no shown). Amphiboles show (Ca + Na) > 1.34 and Na_B < 0.37 and thus are calcic amphibole according to Leake's (1978) classification. The *mg* number [$mg = Mg^{2+}/(Fe^{2+}+Mg^{2+})$]

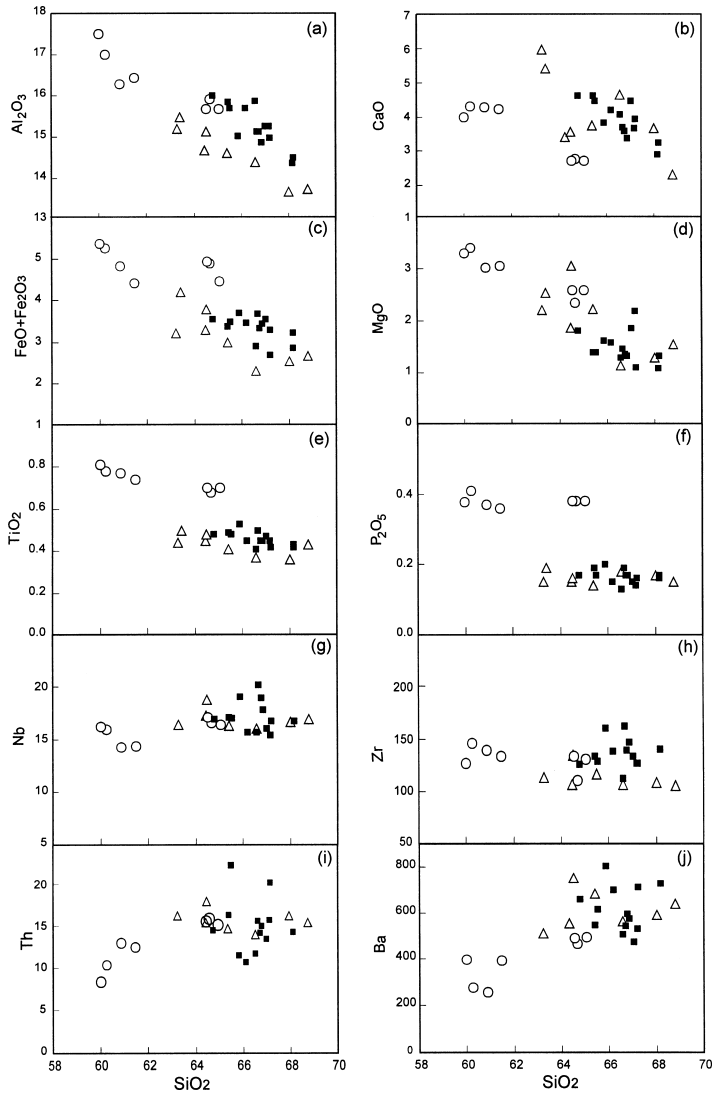

Fig. 4. Variation of major and trace elements against SiO_2 for the diorites-granodiorites in the SHB. Symbols as in Fig. 3(b).

in amphiboles ranges from 0.35 to 0.44. Most hornblendes have a Ti content (cation per 23 oxygens) of <0.15. The mineral assemblage and amphibole composition from the SHB are suitable for the application of the Al-hornblende barometer (e.g., Schmidt, 1992). The calculation result shows that the pressure from these diorites-granodiorites in SHB is in the range of 2.9–4.2 kb, corresponding to a depth of *ca*. 10–13 km under the static pressure condition. The temperatures of *ca*. 800–850°C are obtained using the thermometer of Holland and Blundy (1994) with estimates from Schmidt's geobarometer as pressure input. These results are consistent with the formation temperature of diorites-granodiorites obtained by the application of saturation equations for Zr, LREE and P_2O_5 (e.g., Watson and Harrison, 1983; Montel, 1993).

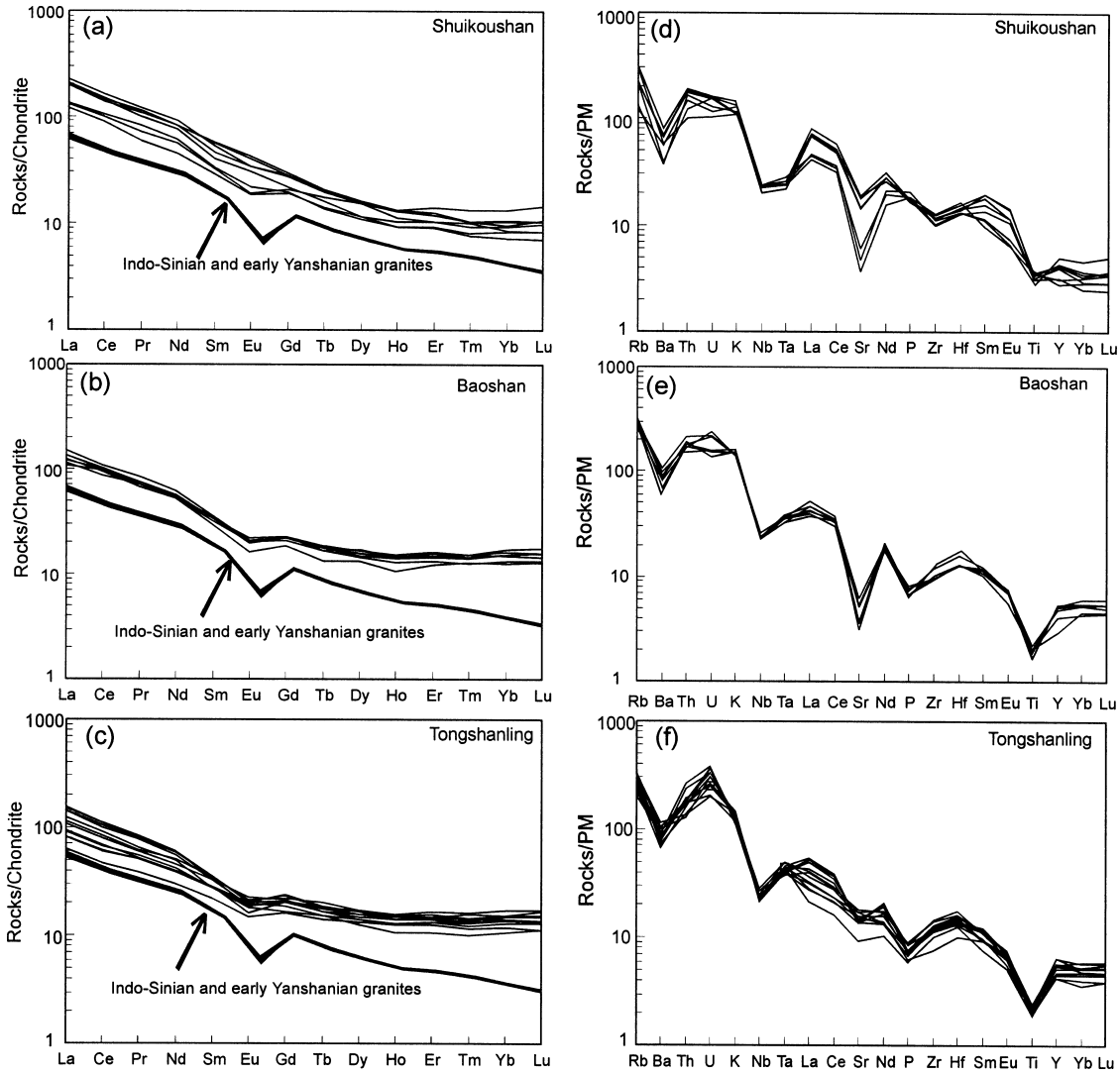

Fig. 5. Chondrite-normalized REE patterns (a)–(c) and primitive mantle-normalized spidergrams of these diorites-granodiorites in the SHB (d)–(f). Normalized values for primitive mantle are from Sun and McDonough (1989) and chondrite from Taylor and McLennan (1985).

Geochemistry

All these samples are high in K_2O content (3.26 to 4.81%) with K_2O/Na_2O ratio of 1.07~2.01. In the SiO_2-K_2O plot, they plotted in the high-K calc-alkaline rock field (Fig. 3(a)) (Morrison, 1980). Baoshan and Tongshanling samples are metaluminous (A/CNK = 0.79–1.01) whereas Shuikoushan samples are slightly peraluminous (A/CNK = 0.98–1.19) in terms of classification schema of Maniar and Piccoli (1989). In the QAP diagram (Fig. 3(b)), Shuikoushan samples lie within diorite and quartz diorite field, whereas Tongshanling and Baoshan samples are almost within granodiorite field (Steckeisen, 1973).

FeO + Fe_2O_3, MgO, CaO and Al_2O_3 contents of these diorites-granodiorites in SHB decrease regularly with increasing SiO_2. TiO_2 and P_2O_5 have little varieties in each intrusion (Figs. 4(a)–(f)). However, Shuikoushan samples have relatively lower SiO_2 but higher MgO, FeO + Fe_2O_3,

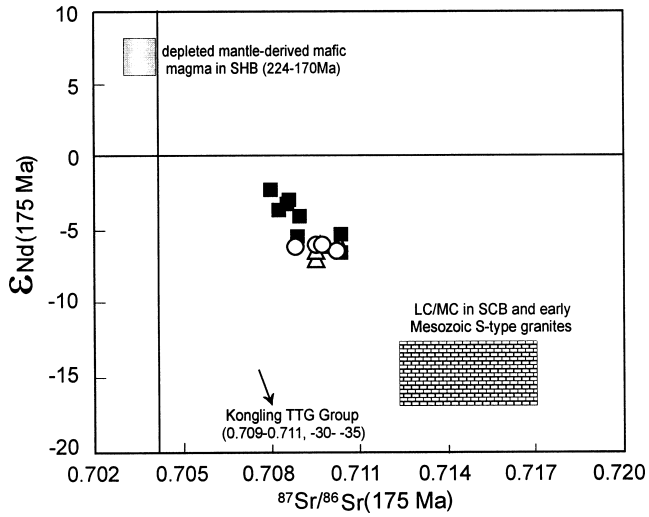

Fig. 6. $^{87}Sr/^{86}Sr(t)$ *vs.* $\varepsilon_{Nd}(t)$ *diagram of early Mesozoic diorites-granodiorites in the SHB, showing that these samples are isotopically different from their neighbouring early Mesozoic S-type granites. Data sources: LC/MC in SCB (Guo et al., 1997b; Li, 1990); early Mesozoic S-type granites (Chen and Jahn, 1998; Shen et al., 1998); lower crust of the Yangtze block represented by Kongling TTG rocks (Gao et al., 1999); depleted mantle-derived mafic magma in SHB (224–170 Ma) (Guo et al., 1997a; Zhao et al., 1998). Symbols as in Fig. 3(b).*

Al_2O_3, TiO_2, P_2O_5 and compatible element contents (Ni, Co and Sc) than Baoshan and Tongshanling samples (Table 3). For Shuikoushan samples, HFSEs (e.g., Zr, Nb) have limited variations (Zr = 111~245 ppm and Nb = 14.2~17.1 ppm), but LILEs (e.g., Th, Ba) have a relatively large range in concentration and generally increase with increasing SiO_2 (Figs. 4(g)–(j), Table 3). In contrast, Baoshan and Tongshanling samples have a small range of HFSEs and LILEs abundance irrespective of SiO_2 contents (e.g., Th, Ba, La, Sr, Zr, Nb), suggesting that magma differentiation plays a less important role during magma evolution.

All these samples have LREE-enriched chondrite-normalized REE patterns and show a slightly HREE fractionated with weakly negative or inappreciable Eu anomalies (Figs. 5(a)–(c)). It is noted that Shuikoushan samples have higher $(La/Yb)_{cn}$ and $(Gd/Yb)_{cn}$ ($(La/Yb)_{cn}$ = 8.96~27.0, $(Gd/Yb)_{cn}$ = 2.01~3.26) than those for Baoshan and Tongshanling granodiorites ($(La/Yb)_{cn}$ = 4.31~12.53, $(Gd/Yb)_{cn}$ = 1.15~1.74). This pattern is significantly different from that of neighbouring Mesozoic S-type granites that show moderate HREE fractionation but strongly negative Eu anomalies (Zhuang *et al.*, 1988).

In the primitive mantle-normalized spidergrams (Figs. 5(d)–(f)), these samples have strong negative Ba, Nb and Ta anomalies and significant enrichment in Rb and LREE. Negative P, Ti and Sr anomalies are also present but extent of the anomalies varies greatly. Negative Sr anomaly in Baoshan samples is more obvious than that in Shuikoushan and Tongshanling samples. Negative P and Ti anomalies for Baoshan and Tongshanling samples, are more significant than those for Shuikoushan samples.

The initial Sr and Nd isotopic ratios have been corrected using an average age of 175 Ma. As illustrated in Fig. 6, all studied samples are plotted in the enriched mantle quadrant. They are isotopically distinct from Indo-Sinian to early Yanshanian granites, metamorphic basement rocks in the SCB and the lower crust in the Yangtze block (Chen and Jahn, 1998; Shen *et al.*, 1998; Guo *et al.*, 1997b; Li, 1990; Gao *et al.*, 1999). Shuikoushan and Baoshan samples have similar

isotopic composition with $^{87}Sr/^{86}Sr$ ratios ranging from 0.708787 to 0.710272 and ε_{Nd} value from –6.98 to –5.90. Tongshanling samples show a relatively wide range of $^{87}Sr/^{86}Sr$ ratio (0.707962~0.710396) and ε_{Nd} value (–6.57~–2.30).

PETROGENESIS

Negative Nb-Ta anomalies are usually regarded as a signature of subduction-related and/or crust-derived magmas (Whalen *et al.*, 1996). The SHB magmas are characterized by significant negative Nb-Ta anomaly (Nb/La = 0.30–0.85), high abundance of incompatible elements, low ε_{Nd} (ε_{Nd} = –6.98 to –2.30) and relatively high $^{87}Sr/^{86}Sr$ ratio (0.707962–0.710396). These characteristics are therefore indicative of involvement crustal components either in the source region of magmas or assimilated by crustal material during its ascent to the surface. Three petrogenetic models can be put forward to explain the elemental and isotopic composition of the diorites-granodiorites in SHB. These include (1) anatexis of crustal rocks (e.g., McDermott *et al.*, 1996); (2) derivation from a mantle source, subsequently by assimilation-fractional crystallization (AFC) processes; and (3) partial melting of underplated basalts hybridized by old crust materials. Evaluation of these alternatives will be the focus of the following discussion.

Anatexis of crustal rocks?

High-K calc-alkaline diorites-granodiorites can be generated by anatexis of the metapelitic assemblage and crustal rocks due to unrooting of a thickened lithosphere or slab break-off (e.g., von Blanckenburg *et al.*, 1998; Altherr *et al.*, 2000). Compositional differences of magmas produced by partial melting of different source rocks under variable melting conditions could be visualized in term of Al_2O_3/(MgO+FeO*) and CaO/(MgO+FeO) ratios (e.g., Altherr *et al.*, 2000). Generally, mantle-derived melts have lower Al_2O_3/(MgO+FeO*) but higher CaO/(MgO+FeO*) than those from metapelitic rocks. As shown in Fig. 7, most of diorites-granodiorites in SHB are plotted in the range of melts derived from a basaltic source.

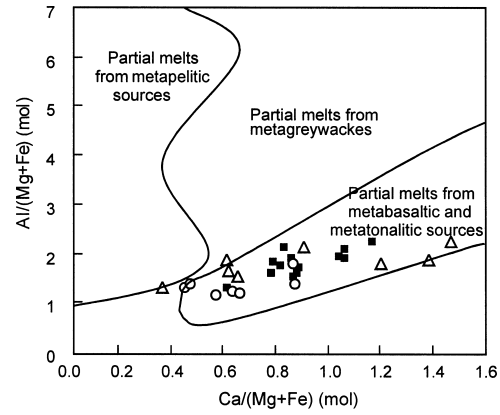

Fig. 7. Al/(Mg+Fe$_{total}$ in molecular ratio) vs. Ca/(Mg+Fe$_{total}$ in molecular ratio) plots of the diorites-granodiorites in SHB, indicating basaltic rocks as their melting source rather than metapelitic rocks. The variation ranges of different sources are from Altherr et al. (2000). Symbols as in Fig. 3(b).

The geochemical signatures and isotopic ratios of these diorites-granodiorites from the SHB (e.g., $^{87}Sr/^{86}Sr(t)$ = 0.707962~0.710396, $\varepsilon_{Nd}(t)$ = –6.98~–2.30 and $\delta^{18}O$ = +8.6~+10.7‰) are different from Precambrian metamorphic basement and their derivative S-type granites in SCB ($^{87}Sr/^{86}Sr(t)$ = 0.7100~0.7250, $\varepsilon_{Nd}(t)$ = –12~–16 and $\delta^{18}O$ = +11.4~+15.0‰) (Zhuang *et al.*, 1988; Li, 1990; Shen *et al.*, 1998). This means that these diorites-granodiorites from the SHB cannot directly originate from Precambrian metamorphic rocks. Hornblende-titanite granodiorites derived from a non-pelitic source would have generally lower Rb/Ba (<0.33) and Rb/Sr (<1.1) ratios than those from metapelitic rocks (Jung *et al.*, 2000). The diorites-granodiorites in the SHB have Rb/Sr and Rb/Ba ratios of 0.80–1.2 and 0.25–0.35, respectively. These observations rule out the upper/middle crustal rocks as sole source for the SHB magmas.

Mafic granulite xenoliths from late Mesozoic alkaline basalts in SHB (Fig. 1(b)) are the direct samples of the lower crust in the SHB (Kong *et*

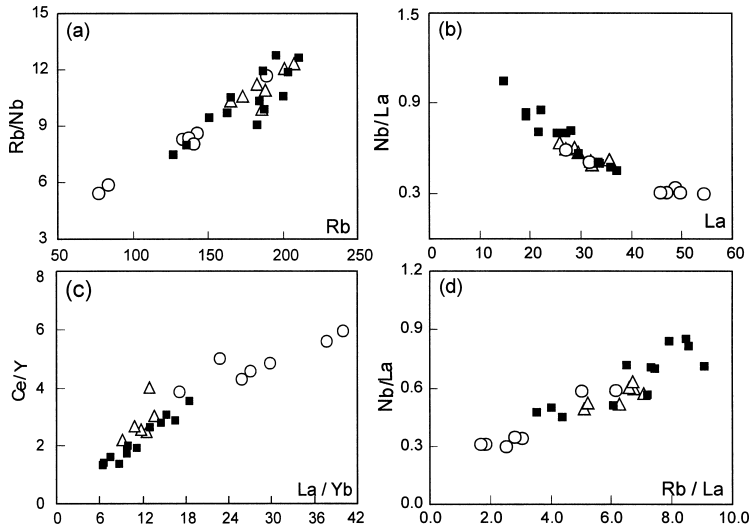

Fig. 8. Element vs. elemental ratio ((a) and (b)) and elemental-elemental ratios ((c) and (d)) of the diorites-granodiorites in the SHB. Symbols as in Fig. 3(b).

al., 2000). They have ε_{Nd} value (ε_{Nd} = –5.8~–6.0 at 175 Ma) (Kong *et al*., 2000) similar to Shuikoushan and Baoshan samples but lower than Tongshanling samples (Fig. 11). Even if such granulite xenoliths are assumed as source materials, and Ca-plagioclase and hypersthene were retained in source during melting, the melting products would possess significantly negative Eu anomalies. However, only weakly negative to inappreciable Eu anomalies are observed in the diorite-granodiorites in the SHB. In addition, experimental studies (e.g., Rushmer, 1991; Sen and Dunn, 1994; Rapp and Watson, 1995) have shown that, regardless of the degree of partial melts, metaluminous to slightly peraluminous intermediate melts, even some mafic melts, by dehydration melting of mafic granulites under extremely high temperature are generally characterized by low K_2O and high Na_2O concentrations (>4.3wt%). However these characteristics are not observed in these diorites-granodiorites in the SHB. On the other hand, most of diorites-granodiorites from the SHB show weakly fractionated HREE, and high Y contents (>18 ppm) as well as relatively low ratios of Sr/Y (3–16). In this regards, they are completely different from the adakitic rocks derived from lower crust, further suggesting that residual garnet was not be involved during the melting process (Martin, 1999). Therefore, derivation of these diorites-granodiorites from mafic granulites alone seems unlikely.

Mantle-derived magma?

As illustrated in Fig. 6, Sr-Nd isotopic compositions of the SHB dioritic-granodioritic magmas can be explained by mixing between the depleted mantle and the middle/lower crust. It is thus possible that these dioritic-granodioritic magmas were derived from an asthenosphere mantle and were subsequently affected by AFC processes during its ascent to the surface. This hypothesis seems to be consistent with the covariance between incompatible elements and elemental ratios (e.g., Rb vs. Rb/Nb) (Figs. 8(a) and (b)) as well as between elemental ratios (e.g., La/Yb vs. Ce/Y and Rb/La vs. Nb/La) (e.g., Langmuir *et al*., 1978; Figs. 8(c) and (d)). One component that exhibits low La but high Nb/La, Rb/Nb ratios is of similar affinity to that of a depleted mantle source or its derivative melts. Another component has high La contents but low Nb/La, Rb/Nb ratios and it might

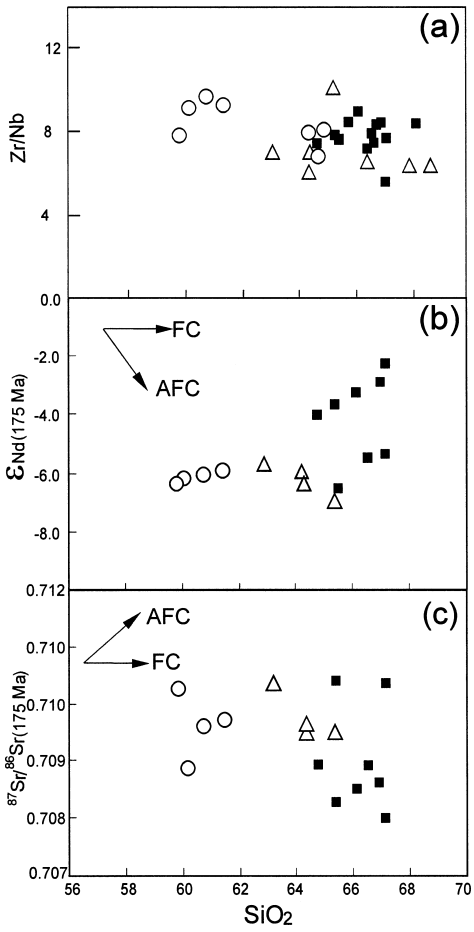

Fig. 9. SiO_2 vs. Zr/Nb (a), $\varepsilon_{Nd}(t)$ (b) and $^{87}Sr/^{86}Sr(t)$ (c) plots of the diorites-granodiorites in the SHB. Symbols as in Fig. 3(b).

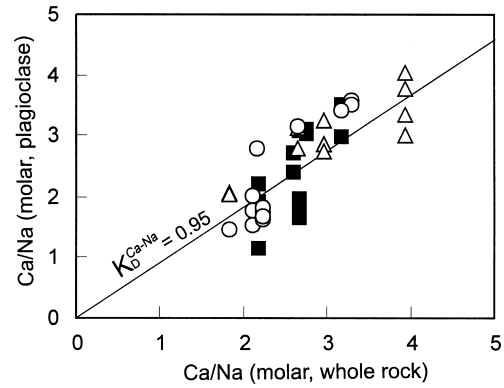

Fig. 10. Plagioclase Ca/Na_{plag} vs. whole-rock Ca/Na (molar) from the diorites-granodiorites in the SHB. Symbols as in Fig. 3(b).

be related to the crust or its derivative melts. Contamination by SiO_2- and K_2O-rich crust materials or mixing by a crust-derived melt during magma ascent would lead to the increase in K_2O/TiO_2 and K_2O/P_2O_5 in magmas. Since Precambrian basement rocks and their derivative melts have higher $^{87}Sr/^{86}Sr$, Zr/Nb and lower ε_{Nd} value, Zr/Nb and $^{87}Sr/^{86}Sr(t)$ of magmas are expected to increase with increasing SiO_2 during crustal contamination (DePaolo, 1981). However, the facts as following do not support the significant crustal contamination: (1) the samples from each intrusion show a very limited variation in K_2O/P_2O_5 and K_2O/TiO_2 (Table 3); (2) the incompatible element ratios, e.g., Zr/Nb, are also relatively constant irrespective of SiO_2 contents (Fig. 9(a)); (3) there is no significantly regular correlation for the samples from each intrusion, as illustrated in the plot of $^{87}Sr/^{86}Sr$ and ε_{Nd} vs. SiO_2 (Figs. 9(b) and (c)).

Compositions of plagioclase and whole rock are shown in Fig. 10. $K_D^{Ca\text{-}Na}$ values for plagioclase-melt exchange equilibrium defined as $(Ca/Na)_{plag}/(Ca/Na)_{liq}$ by Sisson and Grove (1993), has a narrow variation ($K_D^{Ca\text{-}Na}$ = 0.95 in average), similar to the experimental works at 8–10 kb that carried out by Sisson and Grove (1993). This suggests that whole-rock composition is in equilibrium with phenocryst and the system was in a relatively undisturbed state during magma evolution (Hunter and Bleak, 1995). The narrow compositional variations, together with the low An number and normal zoning patterns within plagioclase phenocrysts are inconsistent with mixing between a hot mafic and a cool felsic melts.

Alternatively, the crustal signatures in the SHB magmas may directly inherit from that of an enriched lithospheric mantle. In this case, the relatively high SiO_2 contents (60–68 wt%) and low Mg# (0.40–0.59) in the SHB magmas require a significant fractionation of mafic minerals in magma evolution. However, the common mafic phases in mantle-derived magmas such as olivine and pyroxene are not observed in these diorites-granodiorites from the SHB. Moreover, the slightly fractionated REE patterns and limited

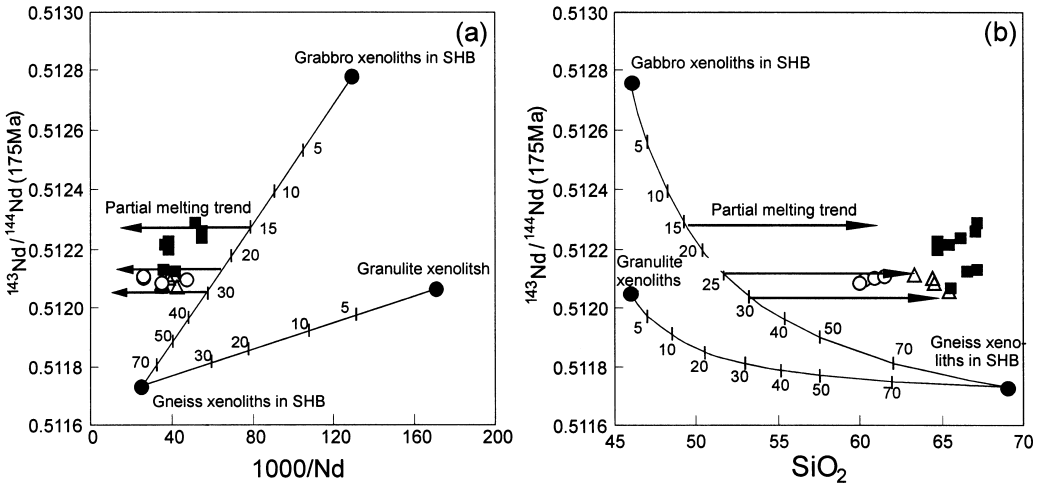

Fig. 11. 1000/Nd and SiO_2 vs. $^{143}Nd/^{144}Nd(t)$ diagrams. The numbers indicate the percentages of participation of the LC/MC rocks. The calculation parameters of Nd (ppm), SiO_2 (wt%) and $\varepsilon_{Nd}(t)$ are 6, 46, –6 for granulite xenoliths in the SHB, 45, 69, –13 for gneiss xenoliths in the SHB, and 8, 46, +6 for gabbro xenoliths in the SHB, respectively (Li, 1990; Shen et al., 1998; Guo et al., 1997a, b; Zhao et al., 1998). The results show that these diorites-granodiorites in the SHB were impossibly generated by the melting of granulites. In contrast, they should be originated from the variable degree partial melting of a hybridized source between 15–30% Precambrian crust (represented by gneiss xenoliths in SHB) and 70–85% early Mesozoic depleted mantle-derived melts (represented by gabbro xenoliths in SHB). Symbols as in Fig. 3(b).

variations in compatible elements (i.e., Ni, Co, Sc and V) argue against a significant fractionation of hornblende in Shuikoushan samples, although a small amount fractionation of hornblende did take place for Baoshan and Tongshanling samples given the negative correlation between SiO_2 and MgO, FeO. A minor role of biotite and alkaline feldspar during the fractionation is inferred from the fact that Ba, Th and Rb increase with increasing SiO_2 for Shuikoushan samples and that the Sr, Ba, Rb, Th concentrations irregular varied with the increasing SiO_2 for Baoshan and Tongshanling samples. On the other hand, the contemporaneous mafic lavas in the SHB has a ε_{Nd} value of +3~+6 (Zhao *et al.*, 1998), and a few gabbro xenoliths with age of *ca*. 224 Ma and peridotite xenoliths have ε_{Nd} value of +5~+8 and +10~+13, respectively (Guo *et al.*, 1997a). This suggests that lithospheric mantle might be depleted rather than enriched before or during the formation of early Mesozoic diorites-granodiorites in the SHB. It is therefore concluded that the geochemical and Sr-Nd isotopic variation for the diorites-granodiorites from the SHB cannot be viably accounted for by crust contamination (or magma mixing) of asthenospheric melts nor by crystal fractionation of an extensive enriched lithospheric mantle-derived melt.

Melting of a hybridized source between underplated basalts contaminated by old crust material?

While the possibility of mantle-derived magma petrogenesis is ruled out, the mixing trends illustrated in Figs. 6 and 8 strongly suggest participation of a mantle component in the genesis of the SHB magmatism. The simplest interpretation is that these dioritic-granodioritic magmas in the SHB were derived from a hybridized source between a mantle-derived magma and an old crust basement. The early Mesozoic mantle-derived magma poorly outcropped in the SHB exclusively exhibit the geochemical characteristics of depleted mantle-derived magma (MORB/OIB) (Guo *et al.*, 1997a; Zhao *et al.*, 1998). The gabbro xenoliths hosted by alkali basalts in the SHB, the important

element of early Mesozoic mantle-derived magma, have lower La but higher Nb/La (0.80–1.20) and ε_{Nd} value (*ca*. +5~+8), similar to those of MORB/OIB (Guo *et al*., 1997a; Kong *et al*., 2000). The gneiss xenoliths hosted by alkali basalts in the SHB, which is usually considered to be equivalent with the component of the LC/MC in South China (Guo *et al*., 1997b; Li, 1990), have lower Nb/La ratio (0.15–0.48, average of 0.30), ε_{Nd} value (*ca*. –13) but higher La content (e.g., Guo *et al*., 1997b; Kong *et al*., 2000; Wang *et al*., unpublished data). Therefore, to define the respective contribution to the crustal and mantle-derived components in the dioritic-granodioritic melt generation, mixing calculations have been performed using the gabbro and gneiss xenoliths in the SHB as two potential components.

The modeling results, shown in Fig. 11(a), suggest that addition of about 25–30% crust component into depleted mantle-derived mafic melts can nicely account for the Sr-Nd isotopic variation for Shuikoushan and Baoshan samples. A slightly low percentage of crustal material (15–30%) was involved for Tongshanling granodiorites. Similar results were obtained by mass balance calculation (Fig. 11(b)). An involvement of *ca*. 15–30% crust material could also better explain the arc-type trace element signatures for these diorites-granodiorites. For example, the variation of Nb/La ratio (0.30–0.85) for these diorites-granodiorites in the SHB could be arrived by those of 15–30% gneiss (Nb/La = 0.15–0.48) and 70–85% gabbro xenoliths (Nb/La = 0.80–1.20).

It is noted from Fig. 11 that all of the rocks in the SHB are plotted along partial melting trend rather than the mixing curve. Therefore, the simple mixing could not produce these diorites-granodiorites in the SHB. Either partial melting to various extents or fractional crystallization controlled redistribution of Nd, SiO_2 and other elements between melt and relict phases. Due to an insignificant role of fractional crystallization process during magma evolution as discussed previously, various degrees of partial melting of a hybridized source may play an important role in generating the major and trace element variations.

Usually, the extent of LREE and REE fractionation (e.g., La/Sm, Ce/Yb) is sensitive to variable degrees of partial melting and to source difference. The shifts in $^{87}Sr/^{86}Sr$ and $^{143}Nd/^{144}Nd$ ratios may be related to the variation of the source compositions (e.g., Giannetti and Ellam, 1994). Shuikoushan samples exhibit higher Ce/Yb (34.5–70.9) than other intrusions (12.3–34.0) but similar La/Sm ratio (4.15–7.63). However, the generally positive correlation for each intrusion between $^{87}Sr/^{86}Sr$ and La/Sm, Ce/Yb ratios clarify that source heterogeneity has a more important contribution to compositional variation in the dioritic-granodioritic magma (Table 3). Therefore the trace elemental and isotopic variation of these diorites-granodiorites in the SHB should be inherited from heterogeneities within the hybridized source region, combined with variable degrees of partial melting. For example, Tongshanling samples with higher ε_{Nd} value have smaller the addition of crust in the source, and their melts contain relatively lower SiO_2, LREE, LILE but high MgO and compatible element contents in comparison with those lower ε_{Nd} samples (Table 3).

TECTONIC IMPLICATIONS

The early Mesozoic tectonic evolution in SCB has been long debated. Some hypotheses, such as Andean-type active continental margin, Alps-type collisional belt, and lithosphere subduction with underplating of mafic magma (e.g., Hsü *et al*., 1990; Faure *et al*., 1996; Zhou and Li, 2000), have been proposed. These hypotheses emphasize the role of either westward subduction of ancient Pacific plate or of the closure of the oceanic basin in the interior of SCB. However, paleomagnetic evidence showed that the westerly-dipping subduction of Pacific plate existed no earlier than 25 Ma (e.g., Engebretson *et al*., 1985). The westward thrust-fault and younger granitoids from west (east of Yangtze Block) to coastal zone (Zhejiang-Fujian provinces) with more than 1000 km in width in the interior of SCB cannot also be solely explained by the westward subduction of ancient Pacific plate (e.g., Li, 2000). The oceanic- or arc-conti-

nental subduction/collision model has also been challenged by the absence of contemporaneous Alps-type tectonic nappes, ophiolite suites, oceanic sedimentary basins and typical arc-island granitoids as well as related paleobiologic assemblage during early Mesozoic. Additionally, geochemical and isotopic data of Mesozoic magmatism indicate an intra-plate tectonic evolution since early Mesozoic, probably Paleozoic (e.g., Rowley *et al*., 1989; Li, 2000; Guo *et al*., 1997a; Zhao *et al*., 1998; Chen and Jahn, 1998).

The NE-trending potassium-rich calc-alkaline diorites-granodiorites in the SHB have arc-type trace element signature and relatively high $^{87}Sr/^{86}Sr$ and lower ε_{Nd}. They may have originated from partial melting of a hybridized source of underplated basalts with old crust material. We therefore suggest that the high-K diorites-granodiorites in the SHB were generated by asthenospheric upwelling in response to the lithospheric extension/thinning under a tensional regime rather than in a subduction zone. This model is similar to those proposed for high-potassium calc-alkaline magmatism in North American and Lachlan fold zone in southeast Australia (e.g., Leat *et al*., 1988; Hawkesworth *et al*., 1995). Li *et al*. (1999) documented some intra-plate shoshonites with emplacement age of 160–170 Ma from southeastern Guangxi Province, which have no Nb-Ta anomalies and relatively high ε_{Nd} value (–2~+3). Therefore, there may exist an important high-ε_{Nd} and low-T_{DM} potassium-rich zone within the SCB, of which diorites-granodiorites in the SHB and shoshonites in southeastern Guangxi Province are the important constituents (Fig. 1(a)). It is noted that extension-related mafic magmatism is sporadically distributed in the interior of South China. This includes 170–180 Ma OIB-type basalt in the SHB, intra-plate shoshonites (~165 Ma) in southeastern Guangxi and western Guangdong Provinces and the bimodal volcanic rocks (~175 Ma) in southern Jiangxi Province (e.g., Wang *et al*., 2001; Zhao *et al*., 1998; Li *et al*., 1999). It is thus inferred that an important intra-continental extensional event occurred not only in SHB, but also in other areas in SCB during early Mesozoic.

These diorites-granodiorites with age of *ca*. 175 Ma in the SHB were derived from a hybridized source as discussed previously. This implies that the generation of dioritic-granodioritic magmatism took place in two consecutive steps that might be closely related to extensional episodes during early Mesozoic.

In the first stage, the basaltic melts were underplated into the lower/middle crust under lithospheric extension setting. A hybridized source of depleted mantle-derived magmas with old crust basement was generated. Given the relatively important volume of these intermediate magmas in the SHB, thermal and material transfer from the mantle to surface during early Mesozoic was probably considerable. If this underplating event took place synchronously with the dioritic-granodioritic magmatism (175 Ma), some contemporaneous eruptive rocks are expected to see in the surface unless the middle/lower crust behaved as a very effective density filter. On the other hand, transfer of important volume of hot mantle-derived magma into middle/lower crust may induce anatexis of crust to generate contemporaneous S-type granitic rocks. To our surprise, however, such rocks are poorly documented in the SHB from late Paleozoic to early Yanshanian (Zhuang *et al*., 1988; HBGMR, 1986). The only exception is the rare outcrops of early Mesozoic gabbro xenolithes (*ca*. 224 Ma) in Daoxian County (Guo *et al*., 1997a; Zhao *et al*., 1998). Most S-type granites resulting from anatexis of the crust in SHB were emplaced during late Indo-Sinian (200~230 Ma, $^{87}Sr/^{86}Sr(t)$ = 0.7180~0.7270 and $\varepsilon_{Nd}(t)$ = –11~–17) (Zhuang *et al*., 1988; HBGMR, 1986), significantly older than the dioritic-granodioritic magmatism (175 Ma) in the SHB. We therefore deduce that the basaltic underplating might have occurred at *ca*. 224 Ma.

Lithosphere extension persistently developed till *ca*. 175 Ma. As a consequence, the thermal gradient of the crust became high enough for a hybridized source formed during previous episode started to melt partially. The process gave rise to the formation of these diorites-granodiorites that are highly enriched in LILE and LREE.

CONCLUSIONS

The early Mesozoic dioritic-granodioritic rocks in the SHB were emplaced at 172–179 Ma at a depth of 10–13 km. They show high-K-calc-alkaline characteristics, LREE, LILE enrichment and HFSE depletion as well as slightly enriched Sr and Nd isotopic compositions (initial $^{87}Sr/^{86}Sr$ = 0.707962 to 0.710396 and $\varepsilon_{Nd}(t)$ = –6.98~ –2.30). These geochemical and isotopic features are remarkably different from their neighboring Mesozoic S-type granitic plutons with significantly negative Eu anomalies and highly enriched Sr-Nd isotopic composition, which were interpreted as the remelting products of Precambrian basement. They might be derived from a hybridized source between 70–85% underplated basalts with 15–30% old crust material rather than anatexis of crustal rocks or melting of an enriched lithospheric mantle. The petrogenesis requests extensive thermal and mass transfer from mantle to crust in response to asthenospheric upwelling and lithospheric extension in SHB. In combination with the occurrence of contemporaneous mafic lavas and shoshonites at other areas in SCB, it should be reasonable that an important intracontinental lithospheric extension event occurred in the SHB, even in SCB during or even before early Mesozoic.

Acknowledgments—The authors would like to thank Y. Liu for her assistance of ICP-MS analysis and R. H. Zhang for his help in the Sr-Nd isotope measurement. We are grateful to Prof. Jun-ichi Matsuda, J. C. Zhou and anonymous reviewer for their critical and constructive reviews/comments on this paper. Dr. Yigang Xu and Hongfu Zhang are thanked for constructive comments on the initial manuscript. This study was financially supported by the National Nature Sciences Foundation of China (40002007), the Ministry of Science and Technology of China (G1999043209) and Chinese Academy of Sciences (KZCX2-102, KZCX3-113, KZCX2-SW-117).

REFERENCES

Altherr, R., Holl, A., Hegner, E., Langer, C. and Kreuzer, H. (2000) High-potassium, calc-alkaline plutonism in the European Variscides: northern Vosges (France) and northern Schwarzwald (Germany). *Lithos* **50**, 51–73.

Chen, J. F. and Jahn, B. M. (1998) Crustal evolution of southeastern China: Nd and Sr isotopic evidence. *Tectonophysics* **284**, 101–133.

DePaolo, D. J. (1981) Trace element and isotopic effects of combined wall rock assimilation and fractional crystallization. *Earth Planet. Sci. Lett.* **53**, 189–202.

Engebretson, D. C., Cox, A. and Gordon, R. G. (1985) Relative motions between oceanic and continental plates in the Pacific basins. *Geological Society of America Special Paper* **206**, 1–59.

Faure, M., Sun, Y., Sun, L., Monie, P. and Charvet, J. (1996) Extensional tectonics within a subduction-type orogen: The case study of the Wugongshan dome (Jiangxi Province, southeastern China). *Tectonophysics* **263**, 77–106.

Gao, S., Lin, W. L., Qiu, Y. M., Zhou, L., Hartmann, G. and Simon, K. (1999) Contrasting geochemical and Sm-Nd isotopic compositions of Archean metasediments from the Kongling high-grade terrain of the Yangtze craton: evidence for cratonic evolution and redistribution of REE during crustal anatexis. *Geochim. Cosmochim. Acta* **63**, 2071–2088.

Giannetti, B. and Ellam, R. (1994) The primitive lavas of Roccamonfina volcano, Roman region, Italy: new constraints on melting processes and source mineralogy. *Contrib. Mineral. Petrol.* **116**, 21–31.

Gilder, S. A., Gill, J., Coe, R. S., Zhao, X. X., Liu, Z. W. and Wang, G. X. (1996) Isotopic and paleomagnetic constraints on the Mesozoic tectonic evolution of South China. *J. Geophys. Res.* **107**(B7), 16137–16154.

Guo, F., Fan, W. M., Lin, G. and Lin, Y. X. (1997a) Sm-Nd dating and petrogenesis of Mesozoic gabbro xenolith in Daoxian County, Hunan Province. *Chinese Science Bulletin* **42**, 1661–1663.

Guo, F., Fan, W. M., Lin, G. and Wu, Y. L. (1997b) Petrological characteristics and dating on gneiss xenoliths in Mesozoic basalts in Huziyan, Daoxian region, Hunan Province. *Journal of Changchun College of Geology* **27**, 41–46 (in Chinese with English abstract).

Hawkesworth, C. J., Turner, S., Gallagher, K., Hunter, A., Bradshaw, T. and Roger, N. (1995) Calc-alkaline magmatism, lithospheric thinning and extension in the Basin and Range. *J. Geophys. Res.* **100**, 10271–10286.

HBGMR (1986) *Regional Geology Survey in Hunan Province*. Geological Press, Beijing, 543 pp.

Holland, T. and Blundy, J. (1994) Non-ideal interactions in calcic amphiboles and their bearing on amphibole-plagioclase thermometry. *Contrib. Min-*

eral. Petrol. **116**, 433–447.

Hsü, K. J., Li, J. L. and Chen, H. H. (1990) Tectonic of South China: Key to understanding West Pacific geology. *Tectonophysics* **183**, 9–39.

Hunter, A. G. and Bleak, S. (1995) Petrogenetic evolution of a transitional tholeiitic-Calc-alkaline series: Towada volcano, Japan. *J. Petrol*. **35**, 1596–1605.

Jung, S., Hoernes, S. and Mezger, K. (2000) Geochronology and petrogenesis of Pan-African, syn-tectonic, S-type and post-tectonic A-type granite (Namibia): products of melting of crustal sources, fractional crystallization and wall rock entrainment. *Lithos* **50**, 259–287.

Kong, H., Jin, Z. M. and Lin, Y. X. (2000) Petrology and chronology of granulite xenoliths in Daoxian county, Hunan Province. *Journal of Changchun University of Science and Technology* **30**, 115–119 (in Chinese with English abstract).

Krogh, T. E. (1973) A low contamination method for hydrothermal decomposition of zircon and extration of U and Pb for isotopic aga determinations. *Geochim. Cosmochim. Acta* **37**, 485–496.

Langmuir, C. H., Vocke, R. D., Hanson, G. N. and Hart, S. R. (1978) A general mixing equation with application to Icelandic basalts. *Earth Planet. Sci. Lett*. **37**, 380–392.

Leake, B. E. (1978) Nomenclature of amphiboles. *Am. Mineral*. **63**, 1023–1052.

Leat, P. T., Thompson, R. N. and Morrison, M. A. (1988) Silicic magma derived by fractional-crystallization from Miocene minette, Elkhend Mountain, Colorado. *Mineral Mag*. **52**, 577–586.

Li, X. H. (1990) Preliminary discussion on the genesis of intermediate-basic veins from Zhuguangshan intrusion: constraints from Sr, Nd and O isotopes. *Chinese Science Bulletin* **35**, 1247–1249.

Li, X. H. (2000) Cretaceous magmatism and lithospheric extension in southeast China. *Journal of Asian Earth Sciences* **18**, 293–305.

Li, X. H., Zhou, H. W. and Liu, Y. (1999) Shoshonitic intrusive suite in SE Guangxi: petrology and geochronology. *Chinese Science Bulletin* **44**, 1992–1998.

Liu, Y., Liu, H. C. and Li, X. H. (1996) Simultaneous and precise determination of 40 trace element elements using ICP-MS. *Geochimica* **25**, 552–558 (in Chinese with English abstract).

Maniar, P. D. and Piccoli, P. M. (1989) Tectonic discrimination of granitoids. *Geol. Soc. Am. Bull*. **101**, 65–643.

Martin, H. (1999) Adakitic magmas: modern analogues of Archaean granitoids. *Lithos* **46**, 411–429.

McDermott, F., Harris, N. B. W. and Hawkesworth, C. J. (1996) Geochemical constraints on crustal anatexis: a case study from the Pan-African Damara granitoids of Namibia. *Contrib. Mineral. Petrol*. **123**, 406–423.

Montel, J. M. (1993) A model for monazite/melt equilibrium and application to the generation of granitic magmas. *Chem. Geol*. **110**, 127–146.

Morrison, G. W. (1980) Characteristics and tectonic setting of the shoshonite rock association. *Lithos* **13**, 97–108.

Rapp, R. P. and Watson, E. B. (1995) Dehydration melting of metabasalt at 8–32 kbar: implications for continental growth and crust-mantle recycling. *J. Petrol*. **36**, 891–931.

Rowley, D. B., Ziegler, A. M. and Nie, G. (1989) Comment on "Mesozoic overthrust tectonics in South China". *Geology* **17**, 384–386.

Rushmer, T. (1991) Partial melting of two amphiboles: contrasting experimental results under fluid-absent condition. *Contrib. Mineral. Petrol*. **107**, 41–59.

Schmidt, M. W. (1992) Amphibole composition in tonalite as a function of pressure: an experimental calibration of the Al-in-hornblende barometer. *Contrib. Mineral. Petrol*. **110**, 304–310.

Sen, C. and Dunn, T. (1994) Dehydration melting of a basaltic composition amphibolite at 1.5 and 2.0 Gpa: implications for the origin of adakites. *Contrib. Mineral. Petrol*. **117**, 394–409.

Shen, W. Z., Ling, H. F., Li, W. X. and Wang, D. Z. (1998) Sr and Nd isotope of Mesozoic granitoids in Jiangxi Province. *Chinese Science Bulletin* **43**, 2653–2657.

Sisson, T. W. and Grove, T. L. (1993) Experimental investigation of the role H_2O in calc-alkaline differentiation and subduction zone magmatism. *Contrib. Mineral. Petrol*. **113**, 143–166.

Stacey, J. S. and Kramers, J. D. (1975) Approximation of terrestrial lead isotope evolution by a two-stage model. *Earth Planet. Sci. Lett*. **26**, 207–221.

Steckeisen, A. L. (1973) Classification and nomenclature of plutonic rocks: recommendation. *N. Jb. Miner. Monat. Jg.*, 149–164.

Sun, S. S. and McDonough, W. F. (1989) Chemical and isotopic systematics of oceanic basalts: implication for mantle composition and processes. *Magmatism in the Ocean Basins* (Sauders, A. D. and Norry, M. J., eds.), *Geol. Soc. Spec. Pub*. **42**, 313–345.

Taylor, S. R. and McLennan, S. M. (1985) *The Continental Crust: Its Composition and Evolution*. Oxford Press, Blackwell, 312 pp.

von Blanckenburg, F., Kagami, H., Deutsch, A. and Oberli, F. (1998) The origin of Alpine plutons along the Periadriatic Lineament. *Schweiz. Mineral Petrol. Mitt*. **78**, 55–66.

Wang, Y. J., Fan, W. M., Guo, F., Li, H. M. and Liang,

X. Q. (2001) U-Pb dating of Mesozoic granodioritic intrusions in southeastern Hunan Province and its petrogenetic implication. *Science in China (series D)* **45**, 271–280.

Watson, E. B. and Harrison, T. M. (1983) Zircon saturation revisited: temperature and composition effects in a variety of crustal magma types. *Earth Planet. Sci. Lett*. **64**, 295–304.

Whalen, J. B., Jenner, G. A., Longstaffe, F. J., Robert, F. and Gariepy, C. (1996) Geochemical and isotopic (O, Nd, Pb and Sr) constraints on A-type granite petrogenesis based on the Topsails igneous suite, Newfoundland Appalachians. *J. Petrol*. **37**, 1463–1489.

Zhao, Z. H., Bao, Z. W. and Zhang, B. Y. (1998) The geochemistry of Mesozoic Basalts in south Hunan Province, South China. *Science in China (series D)* **28** (Suppl.), 7–14.

Zhou, X. M. and Li, W. X. (2000) Origin of Late Mesozoic igneous rocks in Southeastern China: implications for lithosphere subduction and underplating of mafic magmas. *Tectonophysics* **326**, 269–287.

Zhuang, J. L., Liu, Z. W. and Tan, B. X. (1988) Relation of the small rock bodies in southern Hunan to the formation of ore deposits and prognosis of concealed deposits. *Hunan Geology* **4** (Suppl.), 1–163 (in Chinese).